ELSEVIER

International Journal of Heat and Fluid Flow 21 (2000) 359–364

International Journal of
HEAT AND
FLUID FLOW

www.elsevier.com/locate/ijhff

Pressure velocity coupling in a subsonic round jet

C. Picard, J. Delville *

Laboratoire d'Etudes Aérodynamiques, UMR CNRS 6609, Université de Poitiers, CEAT, 43 Route de l'Aérodrome, F-86036 Poitiers, France

Received 23 August 1999; accepted 8 February 2000

Abstract

An experimental investigation involving simultaneous measurements of the radial distribution of velocity within the shear layer of a jet and the longitudinal distribution of pressure surrounding a jet is performed. The use of two statistical approaches (proper orthogonal decomposition, POD and linear stochastic estimation, LSE) permits the analysis, in terms of vortical structures, of the pressure fluctuations surrounding the jet. These structures are found to be responsible for the far-field noise emission. This method thus seems promising for providing a "structural model" of the turbulent flow field. © 2000 Elsevier Science Inc. All rights reserved.

Keywords: Proper orthogonal decomposition; Linear stochastic estimation; Coherent structures; Far-field noise estimation

1. Introduction

In 1952, starting from the momentum and continuity equations of fluid, Lighthill (1952) proposed to consider the sound emitted by a turbulent flow as the solution of an equation governing sound propagation in an acoustic medium containing a distribution of quadrupole sources: the so-called Acoustical Analogy. Then, using the generalized Green's formula, the far-field radiated noise is calculated through a volume integration of sources which are basically the turbulent velocity fluctuations for low Mach number flows. Later, in the early 70s, some authors (Bishop et al., 1971 for example) showed that the large-scale instabilities, which can be interpreted as a coherent structure model, contribute mainly to the jet noise production process.

In order to improve the knowledge of these mechanisms and finally to reduce their influence on the far-field acoustic radiation of high speed hot jets, we try to develop a non-intrusive experimental method of large-scale structure identification adapted to jet flows. Indeed, direct velocity measurement can hardly be obtained in such jets and to overcome these experimental difficulties, we use two approaches. The first one, is based on the proper orthogonal decomposition (POD), first introduced by Lumley (1967) for characterizing the coherent structures (Glauser et al., 1991), and is applied to the near-field hydrodynamic pressure surrounding a jet as performed by Arndt et al. (1997). The second one, first introduced by Adrian (1975), is based on the linear stochastic estimation (LSE) (Cole et al., 1992) and uses the correlation between the fluctuating pressure field and the fluctuating velocity field in a jet as outlined by Arndt and George (1974) and performed in Nithianandan (1980). This leads to a velocity field model useful both in the physical interpretation of the pressure POD modes in terms of structures and in the calculation of the far-field noise induced by the estimated vortical field.

Some results obtained in the simplest case of a subsonic round jet are presented here.

2. Experimental configuration

2.1. Set-up

Experiments are carried out in a round jet with an exhaust velocity $U_j = 15.6$ m/s and a diameter $D = 50$ mm. The radial distribution of both the longitudinal and radial velocity components and the streamwise distribution of the hydrodynamic pressure at the outer edge of the jet mixing layer are measured simultaneously (Fig. 1).

A rake of $N = 16$ condenser microphones (1/4 in. Brüel & Kjaer) is used and aligned at 4.4° relative to the jet axis, following the longitudinal expansion of the jet and located radially close to $y/\delta_\omega = 0.5$, where δ_ω is the local vorticity thickness of the jet shear layer. The microphones are equally spaced and measure the longitudinal distribution of the near-field pressure fluctuations $p(x,t)$, $x \in [D, 5.5 \times D]$. The axial velocity $u(x,y,t)$ and the radial velocity $v(x,y,t)$ are obtained by means of a radially aligned (y direction) rake of 12 X-wires probe (wire length and diameter are 0.7 mm and 2.5 μm). The separation between probes remains constant: $\delta_y = 4$ mm and the rake extent is $0.88 \times D$. Sixteen experiments are performed while the rake of microphones remains at the same location and where the rake of hot-wires is located successively beneath each of the microphones. By this arrangement it becomes possible to relate the space-time evolution of the hydrodynamic pressure to the organized part of the velocity field.

---

* Corresponding author.
E-mail address: joel.delville@lea.univ-poitiers.fr (J. Delville).

PII: S 0 1 4 2 - 7 2 7 X (0 0) 0 0 0 2 1 - 7

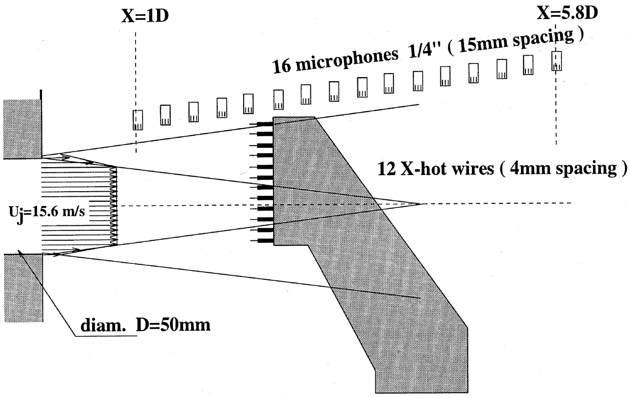

Fig. 1. Sketch of the experimental arrangement.

Particular attention has been paid to the interaction between the rakes. Particularly, spectra and space-time correlations measured with only one rake are found to be quite similar to those measured in the presence of the other rake.

The signal conditioning system is composed of 24 T.S.I.1750 Constant Temperature Anemometers and a microphone polarization unit. The signals are low-pass filtered at 2.5 kHz and are simultaneously sampled at 5 kHz. Thirty acquisition sets of 12k samples are successively performed. The spectral quantities are obtained for 512 frequency points and averaged using 720 records.

2.2. Jet characteristics

From the measured data sets, a first characterization of the shear layer of the turbulent jet is performed. All measured quantities, mean longitudinal velocity field $U(x,y)$ (Fig. 2), Reynolds stress tensor components $\overline{u'^2}(x,y)$, $\overline{v'^2}(x,y)$ and $\overline{u'v'}(x,y)$ (Figs. 3–5) are found in agreement with classical results (Rodi, 1974). Dashed lines in Fig. 2 correspond to the two extreme positions of the hot-wire rake. Note that the rake always covers the jet shear-layer extent. Points outside the rake are plotted using appropriate symmetries.

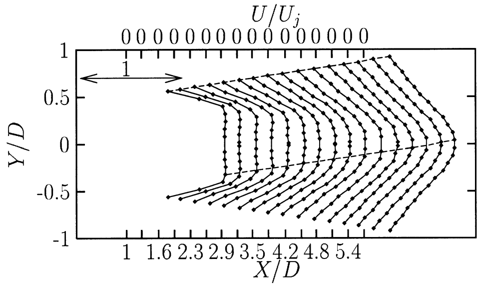

Fig. 2. Mean longitudinal velocity.

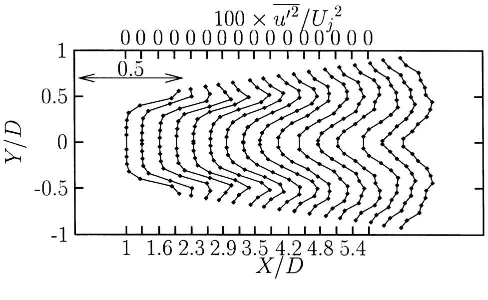

Fig. 3. Mean squared longitudinal velocity fluctuations.

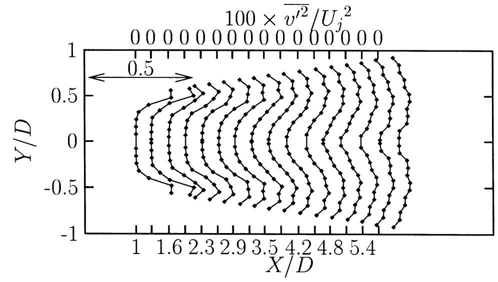

Fig. 4. Mean squared radial velocity fluctuations.

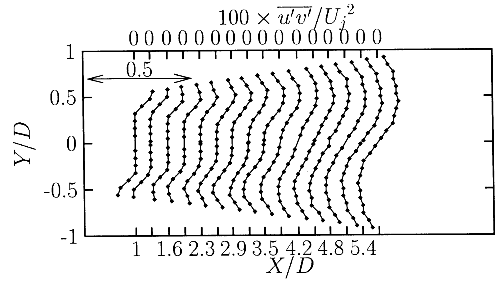

Fig. 5. Mean shear stress.

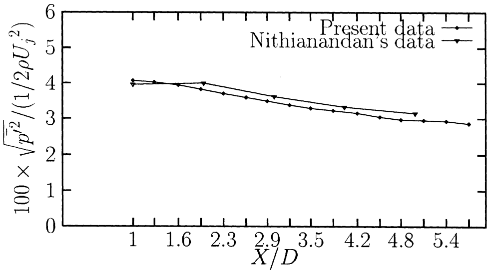

Fig. 6. RMS pressure fluctuations.

The longitudinal decay of the standard deviation of pressure fluctuations plotted in Fig. 6 also follows a classical behavior (Nithianandan, 1980). Typical spectra are plotted in Fig. 7. The pressure spectrum $E_p(f)$ measured at $x/D = 4.5$ exhibits a $f^{-11/3}$ decrease, indicative of the dominance of noise induced by the interaction of turbulence with the mean shear (Jones et al., 1979). The longitudinal velocity spectrum $E_u(f)$ and the radial velocity spectrum $E_v(f)$ measured on the shear layer axis at $x/D = 4.5$ are also plotted in Fig. 7. The inertial subrange ($f^{-5/3}$) covers more than one decade. Spectra E_p and E_v exhibit maxima around $f = 70$ Hz, corresponding to a Strouhal number $St = 2f\delta_\omega/U_j = 0.4$, that is the mark of large-scale structures.

3. Proper orthogonal decomposition

3.1. Generalities

First introduced by Lumley (1967), the POD consists in finding among an ensemble of realizations of the flow field, the realization which maximizes the mean square energy. This leads to a Fredholm integral eigenvalue problem whose kernel

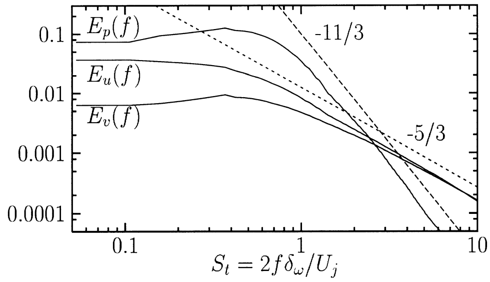

Fig. 7. Typical spectra.

is a two-point cross-correlation tensor. The resolution of the POD problem provides a complete set of orthogonal eigenfunctions which can be interpreted as the most representative realizations of the flow. The POD can be applied only in the directions which are "inhomogeneous". Generally in mixing layers, the POD is applied in the transverse direction y and to velocity (e.g. Delville, 1994). In the present study, the POD is applied, in the longitudinal direction x, to the near-field pressure as in Arndt et al. (1997). From the near-field longitudinal pressure distribution $p(x,t)$ in the jet and its two-point spatial cross-correlation tensor $R_{pp}(x,x')$, the Fredholm equation is written as

$$\int_{D_x} R_{pp}(x,x')\Phi^{(n)}(x')\,\mathrm{d}x' = \Lambda^{(n)}\Phi^{(n)}(x), \tag{1}$$

where $\Phi^{(n)}(x)$ are the real valued eigenvectors at mode n. D_x is the microphone rake extent. Note that $N = 16$ POD modes are obtained. Eigenvalues $\Lambda^{(n)}$ correspond to the energy contained in mode n and form a convergent decreasing series. The overall fluctuating pressure energy is given by the sum of the N eigenvalues. The original fluctuating pressure field can be reconstructed from the eigenfunctions by

$$p(x,t) = \sum_{n=1}^{N} p_p^{(n)}(x,t),$$

where

$$p_p^{(n)}(x,t) = A^{(n)}(t)\Phi^{(n)}(x), \tag{2}$$

with the help of the random projection coefficients

$$A^{(n)}(t) = \int_{D_x} p(x,t)\Phi^{(n)}(x)\,\mathrm{d}x. \tag{3}$$

So, each POD mode contributes independently to the original field through $p_p^{(n)}$. This first application of the POD method is hereafter called physical POD: POD*p*.

Considering the time to be stationary, the kernel of integral equation (1) becomes the two-point cross-spectral tensor $S_{pp}(x,x';f)$ that is the time Fourier Transform of the space-time correlation tensor. The Fredholm equation to be solved is

$$\int_{D_x} S_{pp}(x,x';f)\phi^{(n)}(x';f)\,\mathrm{d}x' = \lambda^{(n)}(f)\phi^{(n)}(x;f). \tag{4}$$

The Fourier Transform $\widehat{p}(x;f)$ of the original field $p(x,t)$ can be reconstructed using

$$\widehat{p}(x;f) = \sum_{n=1}^{N} \widehat{p}_s^{(n)}(x;f),$$

where

$$\widehat{p}_s^{(n)}(x;f) = a^{(n)}(f)\phi^{(n)}(x;f), \tag{5}$$

with

$$a^{(n)}(f) = \int_{D_x} \widehat{p}(x;f)\phi^{*(n)}(x;f)\,\mathrm{d}x, \tag{6}$$

and where the asterisk corresponds to the complex conjugate.

In these last three equations, the eigenvectors and the eigenvalues are frequency dependent and the eigenvectors are complex valued. Note that, due to a phase indetermination problem, the eigenvectors ϕ can be described only in spectral space. This particular application of the POD is hereafter called spectral POD: POD*s*.

There is no direct mathematical relationship between the eigenvectors and the eigenvalues arising from these two types of POD. However, for a given realization of the longitudinal pressure distribution $p(x,t)$, results of the application of these two POD methods can be compared: $p_s^{(n)}(x,t)$ (inverse Fourier Transform of Eq. (5)) and $p_p^{(n)}(x,t)$.

3.2. POD results

A typical space-time sample $p(x,t)$ is plotted in Fig. 8. In this figure, where isovalues are plotted, the horizontal direction corresponds to time $t \in [0, 102]$ ms (from left to right) and the vertical direction corresponds to the streamwise location $x \in [D, 5.5 \times D]$ (from bottom to top). Pressure waves are clearly exhibited by this plot: they are tilted towards the positive time. This inclination can be linked to a global convection velocity. The averaged slope $\mathrm{d}x/\mathrm{d}t \simeq 0.6$ is in agreement with the conventional value of the convection velocity $U_c = 0.6 \times U_j$ in a jet. On the other hand, the noticeable temporal wavelength increase with the downstream location can be related to the spatial expansion of the jet shear layer.

The spatio-temporal evolutions of the first two modes of this sample: $p_s^{(1+2)}(x,t)$ resulting from the POD*s* and $p_p^{(1+2)}(x,t)$ resulting from the POD*p* are, respectively, plotted in Figs. 9 and 10. Clearly by keeping two modes, the spatio-temporal pressure evolution is filtered. For POD*p* and POD*s* as well, the averaged inclination due to convection is preserved. However, the temporal wavelength variation is enhanced by the POD*s* (Fig. 9) while only an averaged wavelength is sorted out by the POD*p* (Fig. 10). The better representation provided by the POD*s* is confirmed by the amount of energy contained in the first mode: 14% and 42% for POD*p* and POD*s* respectively, or contained in the first two modes: 28% and 60%. This indicates that the POD*s* can be a good filter for enhancing the detection of the passage of large-scale structures from the microphone rake signals.

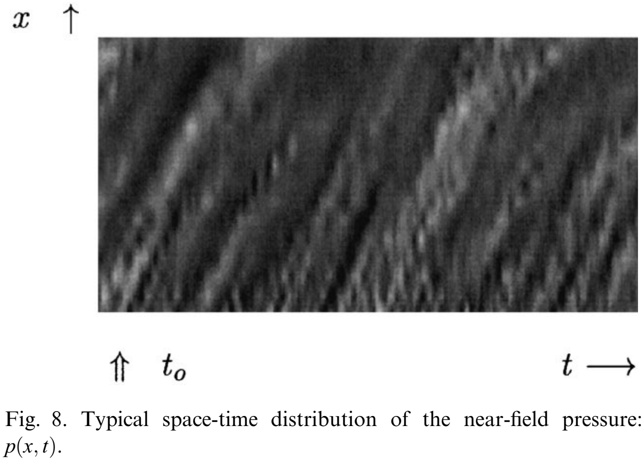

Fig. 8. Typical space-time distribution of the near-field pressure: $p(x,t)$.

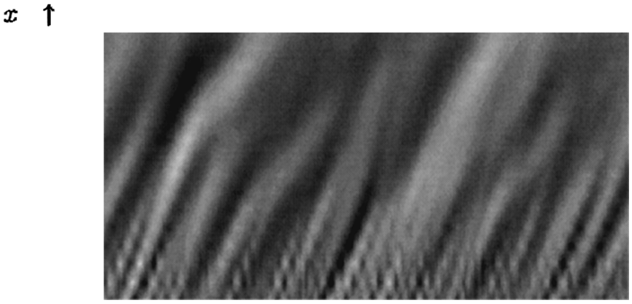

Fig. 9. Contribution of the first two modes of POD$_s$ to the pressure distribution of Fig. 8: $p_s^{(1+2)}(x,t)$.

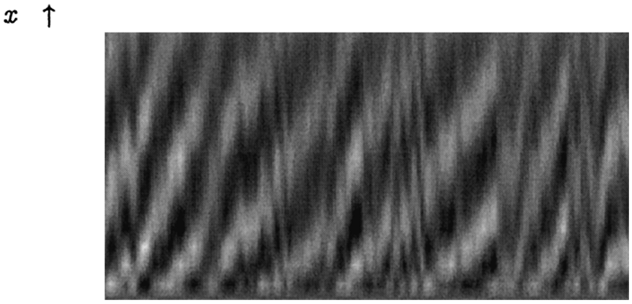

Fig. 10. Contribution of the first two modes of POD$_p$ to the pressure distribution of Fig. 8: $p_p^{(1+2)}(x,t)$.

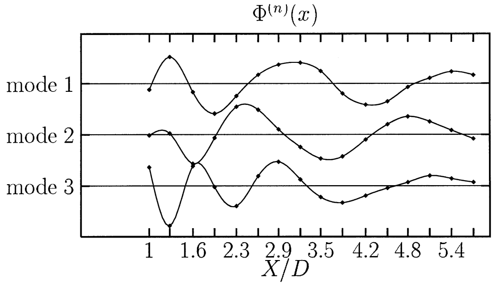

Fig. 11. First three eigenvectors of the physical POD$_p$.

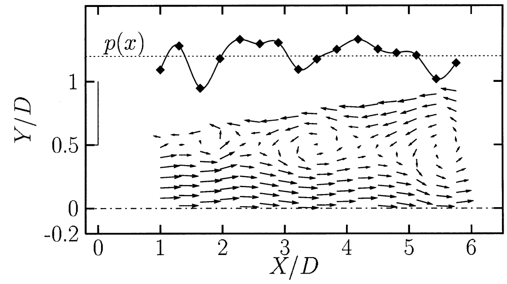

Fig. 12. Estimated velocity vector field induced by the instantaneous pressure distribution (time $t = t_0$ of Fig. 8).

As stated before, due to the phase indeterminacy, no description of the pressure modes can be obtained in the physical space for the POD*s*. The analysis of the modes is then restricted to the POD*p*. The longitudinal evolution of the first three eigenvectors of the POD*p* is plotted in Fig. 11. For all the eigenvectors, the wavelength is increasing with the abscissa x while the amplitude is decreasing. Moreover, the wavelength becomes shorter when the mode number is increasing. The phase difference between the modes 1 and 2 can be related to the structure convection (Aubry et al., 1997).

The next step is to find a physical interpretation of the POD*p* modes in terms of vortical structures.

4. Linear stochastic estimation

In order to relate the longitudinal pressure distribution to the velocity distribution within the shear layer, the LSE can be used. In the present approach, the velocity fluctuations are estimated as a linear combination of the longitudinal fluctuating pressure distribution

$$\begin{aligned}\tilde{u}(x,y,t)&=\sum_{i=1}^{N}A_i(x,y)p(x_i,t),\\ \tilde{v}(x,y,t)&=\sum_{i=1}^{N}B_i(x,y)p(x_i,t),\end{aligned}\tag{7}$$

where x_i correspond to the microphone locations, and (x,y) covers all the shear layer extent. By multiplying this equation by the pressure at location x_j and applying a temporal average, the steady coefficients A_i and B_i can be calculated from the two-point spatial *velocity–pressure* and *pressure–pressure* cross-correlations. This method requires high correlation levels which is the case here. Once the coefficients A_i and B_i are known, the velocities over the whole measurement domain can be estimated simply from the near-field pressure. A typical example of an estimated velocity field is plotted, in a convected frame of reference in Fig. 12, at the given time $t = t_0$ (see Fig. 8). The plotted vectors are

$$\begin{aligned}&\tilde{u}(x,y)+U(x,y)-U_{\mathrm{c}},\\ &\tilde{v}(x,y)\end{aligned}\tag{8}$$

The estimated velocity field corresponds to a succession of aligned vortices whose size increases with downstream distance. Note that the abscissa of the negative pressure peaks coincide exactly with the vortex centers.

In Eq. (7), the pressure $p(x_i,t)$ can be replaced by a physical POD eigenfunction $\sqrt{\Lambda^{(n)}}\Phi_p^{(n)}(x_i)$. The resulting velocity fields are plotted on Figs. 13 and 14 for modes $n = 1$ and 2. The spatial growth of the eigenfunction wavelength, previously observed, is clearly related to the augmentation of the size of the structures. Then the use of the LSE technique provides a physical interpretation of the pressure POD modes. At this stage, a vortical model is available and can be useful to the calculation of the noise generated by the structures.

5. Aeroacoustical results

A physical interpretation of this model can be obtained by calculating the far-field acoustic radiation of the estimated velocity field. As pointed out in Section 1, Lighthill (1952) rearranges the Navier–Stokes equations and expresses the acoustic pressure generated at an observation point $\vec{X}$ through an integration over a turbulence finite volume $\mathscr{V}$ containing the source terms and called in the Lighthill tensor. At low Mach numbers, for isentropic flows, the Lighthill tensor depends only on instantaneous velocities $\rho_0 u_i(t)u_j(t)$. Then the acoustic pressure can be written as

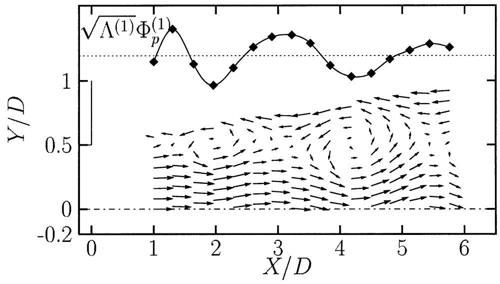

Fig. 13. Velocity vector field induced by the first spatial POD mode.

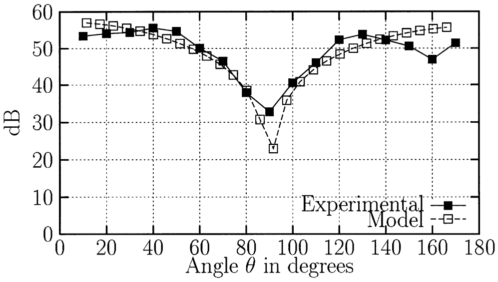

Fig. 15. Directivity at 120*D*.

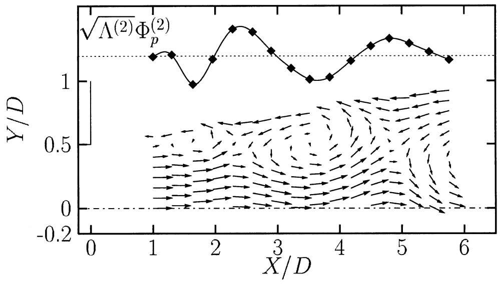

Fig. 14. Velocity vector field induced by the second spatial POD mode.

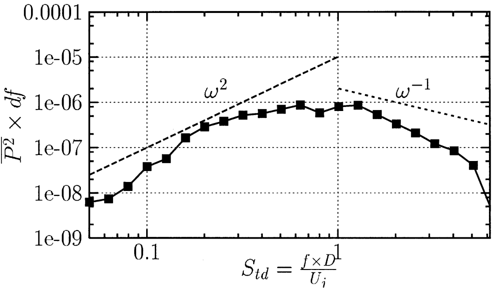

Fig. 16. Estimated 1/3 octave spectral density at $\theta = 90°$ and $|\vec{X}| = 120D$.

$$p(\vec{X},t) = \frac{\rho_0}{4\pi} \int_{\mathcal{V}} \frac{1}{r} \left[\frac{\partial^2 u_i u_j}{\partial y_i \, \partial y_j} \right] \mathrm{d}\vec{Y}, \tag{9}$$

with $r = |\vec{X} - \vec{Y}|$, $\vec{Y}$ is the source point vector and where the terms between brackets are taken at the retarded time $t - r/c_0$. The density ρ_0 and the sound velocity c_0 are those of the fluid at rest.

Lighthill's theory is established for a finite turbulent field containing all the sources and surrounded by a medium at rest. Generally, as in the present case, only a truncated part of the turbulent field is known. Witkowska and Juvé (1994) show for a truncated domain V that the use of the following equation leads to a correct evaluation of the radiated noise

$$p(\vec{X},t) = \frac{\rho_0}{4\pi} \frac{\partial^2}{\partial x_i \, \partial x_j} \int_V \frac{1}{r} [u_i u_j] \, \mathrm{d}\vec{Y}. \tag{10}$$

Starting from 2D slices of the truncated turbulent estimated velocity field

$$\begin{aligned} u_1(\vec{Y},t) &= U(x,y) + \widetilde{u}(x,y,t), \\ u_2(\vec{Y},t) &= V(x,y) + \widetilde{v}(x,y,t), \end{aligned} \tag{11}$$

Eq. (10) is used to calculate the sound generated at a large distance, the third velocity component contribution being neglected. The velocities ($\widetilde{u}$ and $\widetilde{v}$) are estimated with the help of Eq. (7) from the measured near-field pressure distribution.

The instantaneous temporal far-field acoustic pressure is calculated at 17 observation points defined by $|\vec{X}| = 120D$ and $\theta = 10$–$170°$, where θ is the angle between the observation vector $\vec{X}$ and the jet axis. The directivity of the jet (i.e. mean squared pressure in dB, relative to 2×10^{-5} Pa, function of θ) is plotted in Fig. 15. The drop in level around the angle $\theta = 90°$ corresponds to the dominance of the noise due to the interaction of turbulence with the mean shear (called shear noise) over the noise induced by the turbulence itself (called self-noise). The calculated directivity is compared to the shear noise directivity model suggested by Goldstein and Rosenbaum (1973): the mean square pressure is proportional to $(\cos^4\theta + \cos^2\theta)/(1 - M_c \times \cos\theta)^5$, where the convection Mach number $M_c = U_c/c_0$. Clearly, because of the relatively small Reynolds number of the flow under study ($Re = 4.5 \times 10^4$), the self-noise component contributes weakly to the global noise generation process. In fact the spectrum of the near-field pressure given in Fig. 7 already points out this information since the spectral decrease following the $f^{-11/3}$ law is typical of the shear noise.

The good representation of the acoustic phenomena of the estimated field is also illustrated by the 1/3 octave spectral density. A typical spectrum estimation taken at $\theta = 90°$ and $|\vec{X}| = 120D$ is given in Fig. 16. The obtained frequency shape is classical with a maximum around the Strouhal number $St = 1$. Nevertheless, the high frequency behavior (following the ω^{-1} law) indicated by Blake (1986) is not really followed. It may be due to the weak contribution of the self-noise which radiates at higher frequencies than the shear noise.

Actually, the relative contribution of shear noise and self-noise on the global noise emission can only be found by measuring the acoustic far-field. It will determine whether the dominance of the shear noise corresponds to the real acoustic radiation of the jet or to a particular behavior of the model.

6. Conclusions

By measuring simultaneously the longitudinal distribution of the near-field pressure and the radial velocity fluctuations in a jet, a 2D vortical model is obtained. This model allows a physical interpretation, in terms of structures, of the eigenvectors stemming from the POD applied to the pressure distribution. Moreover, the simple measurement of the near-field pressure instantaneous distribution provides an estimate of the temporal evolution of the spatial velocity field. Thus the acoustic far-field generated by these structures can be calculated using the Lighthill equation. It is shown that these structures produce sound which is basically a shear noise. Even if many developments and checks of this method still have to be carried out, it should lead to a promising way of acoustical identification of large-scale structures. In particular, future work will be devoted to the relation between the POD modes of the near-field pressure with the induced far-field noise. Azimuthal dependency will also be investigated.

References

Adrian, R.J., 1975. On the role of conditional averages in turbulence theory. In: Proceedings of the Fourth Biennal Symposium on Turbulence in Liquids. Science Press, Princeton, NJ, p. 323.

Arndt, R.E.A., George, W.K., 1974. Investigation of the large-scale coherent structure in a jet and its relevance to jet noise. In: Proceedings of the Second Interagency Conference on Transportation Noise. North Carolina State University Press, pp. 142–160.

Arndt, R.E.A., Long, D.F., Glauser, M.N., 1997. The proper orthogonal decomposition of pressure fluctuations surrounding a turbulent jet. J. Fluid Mech. 340, 1–33.

Aubry, N., Guyonnet, R., Lima, R., 1997. Spatio-temporal analysis of complex signals: theory and applications. J. Nonlinear Sci. 2, 183.

Bishop, K.A., Fowcs Williams, J.E., Smith, W., 1971. On the noise sources of the unsuppressed high-speed jet. J. Fluid Mech. 50 (591), 21–31.

Blake, W.K., 1986. Mechanics of flow-induced sound and vibration. Applied Math. Mech., vol. 17-I. Academic Press, New York, p. 182.

Cole, D.R., Glauser, M.N., Guezennec, Y.G., 1992. An application of the stochastic estimation to the jet mixing layer. Phys. Fluids A 4 (1), 192.

Delville, J., 1994. Characterization of the organization in shear layers via the Proper Orthogonal Decomposition. Appl. Sci. Res. 53, 263.

Glauser, M.N., Zheng, X., George, W.K., 1991. In: Gatski, Sarkar, Speziale (Eds.), Studies in Turbulence, Springer, Berlin, p. 207.

Goldstein, M., Rosenbaum, B., 1973. Effect on anisotropic turbulence on aerodynamic noise. J. Acoust. Soc. Amer. 54 (3), 630.

Jones, B.G., Adrian, R.J., Nithianandan, C.K., Planchon, H.P., 1979. Spectra of turbulent static pressure fluctuations in jet mixing layers. AIAA J. 17 (5), 449–457.

Lighthill, M.J., 1952. On soung generated aerodynamically I. General Theory Proc. Roy. Soc. London, series A, Mathematical and Physical Sciences, vol. 211, pp. 564–587.

Lumley, J.L., 1967. The structure of inhomogeneous turbulent flows. In: Yaglom, Tatarsky (Eds.), Atm. Turb. Radio Wave Prop. Nauka, Moscow, pp. 166–178.

Nithianandan, C.K., 1980. Fluctuating velocity–pressure fiels structure in a round jet turbulent mixing region. PhD Dissertation, University of Illinois at Urbana–Champaign.

Rodi, W., 1974. In: Launder, B.E. (Ed.), Studies in Convection – Theory, Measurements and Applications, vol. 1. Academic Press, New York, p. 79.

Witkowska, A., Juvé, D., 1994. Estimation numérique du bruit rayonné par une turbulence homogène et isotrope. C. R. Acad. Sci. Paris t. 318 (II), 597–602.